* 9 APR 1948

NATIONAL ADVISORY COMMITTEE FOR AERONAUTICS

TECHNICAL MEMORANDUM

No. 1185

SYSTEMATIC INVESTIGATIONS OF THE INFLUENCE OF THE SHAPE OF THE PROFILE UPON THE POSITION OF THE TRANSITION POINT

By K. Bussmann and A. Ulrich

TRANSLATION

"Systematische Untersuchungen über den Einfluss der Profilform auf die Lage des Umschlagspunktes"
Technische Berichte Band 10, Heft 9, und Vorabdrucke aus Jahrbuch 1943 der deutschen Luftfahrtforschung, IA 010, pp. 1-19

Washington
October 1947

N A C A LIBRARY
LANGLEY MEMORIAL AERONAUTICAL
LABORATORY
Langley Field, Va.

NATIONAL ADVISORY COMMITTEE FOR AERONAUTICS

TECHNICAL MEMORANDUM NO. 1185

SYSTEMATIC INVESTIGATIONS OF THE INFLUENCE OF THE SHAPE OF THE PROFILE UPON THE POSITION OF THE TRANSITION POINT*

By K. Bussmann and A. Ulrich

The position of the beginning of transition laminar/turbulent as a function of the thickness and the camber of the profile at various Reynolds numbers and lift coefficients was investigated for a series of Joukowsky profiles. The calculation of the boundary layer was carried out according to the Pohlhausen method which may be continued by a simplified stability calculation according to H. Schlichting (4). A list of tables is given which permits the reading off of the position of the transition point on suction and pressure side for each Joukowsky profile.

OUTLINE

I. Statement of the problem

II. Extent of the investigation

III. The calculation of the potential velocity and the practical application of the boundary layer and stability calculations:

(a) Potential flow
(b) Boundary layer and stability calculation

---

*"Systematische Untersuchungen über den Einfluss der Profilform auf die Lage des Umschlagspunktes." Zentrale für wissenschaftliches Berichtswesen der Luftfahrtforschung des Generalluftzeugmeisters (ZWB) Berlin-Adlershof, Technische Berichte und Vorabdrucke aus Jahrbuch 1943 der deutschen Luftfahrtforschung, Band 10(1943), Heft 9, Sept. 15, 1943, IA 010, pp. 1-19.

IV. Results:

(a) Influence of the c_a-value and of the Reynolds number
(b) Influence of the camber of the profile f/t
(c) Influence of the thickness of the profile d/t
(d) List of tables for the separation and instability points for all Joukowsky profiles
(e) Mean value of the laminar-flow distance of suction and pressure side for all Joukowsky profiles

V. Summary

VI. References

SYMBOLS

x,y	rectangular coordinates in the plane
s	profile contour length starting from the nose of the profile
t	wing chord
t'	length of the profile contour from nose to trailing edge (different for pressure and suction side)
U_o	velocity of incoming flow
$U_m(s)$	potential velocity at the profile
δ_{P4}	boundary layer thickness according to Pohlhausen P4
δ^*	displacement thickness of the boundary layer
$z_4 = \frac{\delta_{P4}^2}{\upsilon} \frac{U_o}{t}$	nondimensional boundary layer thickness
$\lambda_{P4} = z_4 \frac{t}{U_o} \frac{dU_m}{ds}$	form parameter of the boundary-layer profiles according to Pohlhausen P4

λ_{P6}	form parameter according to Pohlhausen P6
$f(\lambda_{P4})$, $g(\lambda_{P4})$	universal functions of the boundary-layer calculation
$s_{crit.}$	position of the instability point, measured along the contour of the nose of the profile
s_{AP6}	position of the separation point according to P6 method

I. STATEMENT OF THE PROBLEM[1]

The position of the transition point laminar/turbulent in the frictional boundary layer is of decisive importance for the problem of the theoretical calculation of the profile drag of an airfoil since the friction drag depends on it to a high degree. The position of the transition point on the airfoil is largely dependent on the pressure distribution along the contour of the profile and, therefore, on the shape of the airfoil section and on the lift coefficient. A way of theoretical calculation of the start of transition (instability point), that is, the point downstream from which the boundary layer is unstable, was recently indicated by H. Schlichting (1,3,4) and J. Pretsch (2).

According to present conceptions the turbulence observed in tests develops from an unstable condition by a mechanism of excitation as yet little known; therefore, the experimental transition point is always to be expected a little further back than the theoretical instability point.

Knowledge of the theoretical instability point is, nevertheless, important for the research on profiles, in particular for the drag problem. Recently a report

---

[1]An extract of this report was given in a lecture of the first-named author at the Lilienthal meeting for the discussion of boundary-layer problems in Göttingen on October 28 and 29, 1941.

was made about airfoil sections which, due to a position very far back of the instability and transition point, have surprisingly small drag coefficients (laminar profiles). Thus far no systematical investigations of the influence of the shape of the profile upon the position of the transition point have been made either experimentally or theoretically. The following calculation of the theoretical instability point is, therefore, given for the first time in a sufficiently large range of c_a-values and Reynolds numbers to achieve a greater systematization of airfoil sections. In order to keep the extent of calculations within tolerable limits only the two most important profile parameters, thickness and camber were varied. A rather convenient and accurate mode of calculation of the potential flow for the profiles is important for these investigations and the selection of a series of Joukowsky profiles was, therefore, natural. It was not advisable to take for instance the NACA series as a basis; the calculation of the potential flow for such profiles according to the methods at present available does not achieve the accuracy which is required here.

II. EXTENT OF THE INVESTIGATION

A series of ordinary Joukowsky profiles of the relative thicknesses $d/t = 0, 0.05, 0.10, 0.15, 0.20, 0.25$ and the relative cambers $f/t = 0, 0.02, 0.04, 0.08$ were taken as a basis. (See fig. 1.) For instance, J 415 stands for the Joukowsky profile of camber $f/t = 0.04$ and the thickness $d/t = 0.15$. The c_a-region which was examined is $c_a = 0$ to 1 and the Re-number range $Re = \frac{U_o t}{\nu} = 10^4$ to 10^8. The complete calculations were carried out only for the following profiles: 000, 005, 015, 025, 215, 400, 415, 425, 800, 815, and 825. The results for the remaining profiles could be obtained by interpolation. Thus it was possible to obtain a result with tolerable loss of time in spite of the very extensive program (four parameters); a certain amount of accuracy had to be neglected since the interpolation sometimes was carried out over three points.

III. THE CALCULATION OF THE POTENTIAL VELOCITY AND THE PRACTICAL APPLICATION OF THE BOUNDARY LAYER AND STABILITY CALCULATIONS

(a) The Potential Flow

The calculation of the potential velocity with its first and second derivatives along the profile contour forms the basis for a boundary layer and stability calculation. The potential flow about a Joukowsky profile is obtained by conformal mapping of the flow about a circular cylinder. (See fig. 2.)

A short list of the most important symbols and formulas for the profile contour and for the velocity distribution follows:

$$\left.\begin{aligned} z &= x + iy \\ \zeta &= \xi + i\eta \end{aligned}\right\} = \text{Coordinates in the complex plane}$$

mapping function:

$$\zeta = z + \frac{a^2}{z}$$

circle $K_4 \longrightarrow$ mean camber line of the profile

circle $K \longrightarrow$ cambered profile

a radius of the unit circle in the z-plane

R radius of the circle to be mapped in the z-plane

t wing chord

t' length of the profile contour from nose to trailing edge (different for suction and pressure side)

x_o, y_o coordinates of the center of the circle to be mapped in the z-plane (circle K)

o, y_1 center coordinates of the mapping circle of the mean camber line of the profile (circle K_4)

φ varying angular coordinate of the conformal transformation

$-\beta$ zero lift direction (See fig. 2.)

α angle of attack of the airfoil referred to the theoretical chord

α_g geometrical angle of attack referred to the bitangent (See fig. 2.)

Profile nose: $\varphi = \pi + \beta$

Trailing edge: $\varphi = -\beta$

$$\left.\begin{aligned} \frac{x_o}{a} &= \epsilon_1 = \text{thickness parameter; } k = 1 + \epsilon_1 \\ \frac{y_1}{a} &= \epsilon_4 = \text{camber parameter} \end{aligned}\right\} \text{See table I.}$$

$$\beta = \text{arc cos } \frac{1}{\sqrt{1 + \epsilon_4^2}} = \text{arc sin } \frac{\epsilon_4}{\sqrt{1 + \epsilon_4^2}}$$

The profile parameters ϵ_1, ϵ_4, and β can be found in table 1.

Profile contour:

$$\left.\begin{aligned} \frac{x}{t} &= \frac{a}{t}\left[\left(k\sqrt{1 + \epsilon_4^2}\cos\varphi - \epsilon_1\right)\left(1 + \frac{1}{N}\right) + \frac{1 + \left(k + \epsilon_1\right)^2}{k + \epsilon_1}\right] \\ \frac{y}{t} &= \frac{a}{t}\left[k\left(\epsilon_4 + \sqrt{1 + \epsilon_4^2}\sin\varphi\right)\left(1 - \frac{1}{N}\right)\right] \end{aligned}\right\} \quad (1)$$

$$N = k^2\left(1 + 2\epsilon_4^2\right) + \epsilon_1^2 + 2k\sqrt{1 + \epsilon_4^2}\left(-\epsilon_1 \cos\varphi + \epsilon_4 k \sin\varphi\right)$$

$$\frac{t}{a} = 2 + \frac{1 + \left(k + \epsilon_1\right)^2}{k + \epsilon_1} \qquad (1(a))$$

Nose radius ρ/t:

For symmetrical profiles the equation

$$\frac{\rho}{t} = \frac{2\epsilon_1^2}{1 + 2\epsilon_1 + 4\epsilon_1^2} \qquad (2)$$

is valid exactly. This formula may with a good approximation also be applied to cambered profiles. The numerical values in table 1 show that the nose radius of the Joukowsky profiles is only little larger than for the NACA profile family according to NACA report 460 for which $\rho/t = 1.1(d/t)^2$.

Velocity distribution:

$$\frac{U_m}{U_o} = 2\left[\sin(\varphi - \alpha) + \sin(\alpha + \beta)\right] P_1(\varphi) \qquad (3)$$

Stagnation points: Back $\varphi = -\beta$

Front $\varphi = \pi + \beta + 2\alpha$

$$P_1(\varphi) = \frac{N}{\sqrt{(N - 1)^2 + 4k^2\left(\epsilon_4 + \sqrt{1 + \epsilon_4^2}\sin\varphi\right)^2}} \qquad (4)$$

Velocity at the trailing edge:

$$\lim_{\varphi \to -\beta} \left(\frac{U_m}{U_o}\right) = \frac{\cos\,(\alpha + \beta)}{k\sqrt{1 + \epsilon_4^{\,2}}} \tag{5}$$

Arc length:

$$\frac{ds}{d\varphi} = \sqrt{\left(\frac{dx}{d\varphi}\right)^2 + \left(\frac{dy}{d\varphi}\right)^2} \tag{6}$$

s as a function of φ is to be ascertained from (6) by graphical integration or can be seen directly in an enlarged presentation of the profile contour (t = 1m).

Velocity gradient:

$$\frac{1}{U_o}\,\frac{dU_m}{d\varphi} = 2\left\{\frac{N}{N_1^{\,1/2}}\cos\,(\varphi - \alpha) + \frac{B}{N_1^{\,3/2}}\left[\sin\,(\varphi - \alpha) + \sin\,(\alpha - \beta)\right]\right\}$$

$$A = 2k\left(\epsilon_4 + \sqrt{1 + \epsilon_4^{\,2}}\,\sin\,\varphi\right)$$

$$N_1 = (N - 1)^2 + A^2$$

$$B = N_1\,N' - N\left[(N - 1)\,N' + 2k\sqrt{1 + \epsilon_4^{\,2}}\,A\cos\,\varphi\right]$$

$$N' = 2k\sqrt{1 + \epsilon_4^{\,2}}\left(\epsilon_1\,\sin\,\varphi + \epsilon_4 k\cos\,\varphi\right) \tag{7}$$

The first derivative of the potential velocity with respect to the arc length $\frac{dU_m}{ds}$ was calculated numerically from equations (6) and (7), and from that graphically the second derivative $\frac{d^2U_m}{ds^2}$.

Relation between c_a and α:

$$c_a = 8\pi \frac{R}{t} \sin(\alpha + \beta)$$

$$\frac{R}{t} = \frac{k\sqrt{1 + \epsilon_4^2}}{3 + 2\epsilon_1 + \frac{1}{k + \epsilon_1}}$$; compare tables 1 and 2.

(b) Boundary-Layer and Stability Calculation

After calculation of the potential velocity with its first and second derivatives along the profile contour there is a boundary-layer and stability calculation to be made for each profile. The boundary-layer calculation according to Pohlhausen (5) was based upon the differential equation for the boundary layer thickness in the shape indicated by Howarth (6)[2].

$$\boxed{z_4' \equiv \frac{dz_4}{d(s/t)} = \frac{f(\lambda)}{U} + z_4^2 g(\lambda) U'} \qquad (8)$$

---

[2]In the meantime a simpler form of the Pohlhausen equation was indicated by H. Holstein and T. Bohlen (10) where the momentum thickness appears as independent variable. For this method the second derivative U" is unnecessary; the integration procedure is thus simplified considerably.

The following symbols stand for

$$U \equiv \frac{U_m}{U_o}, \quad U' \equiv \frac{t}{U_o}\frac{dU_m}{ds}, \quad U'' \equiv \frac{t^2}{U_o}\frac{d^2U_m}{ds^2},$$

δ_{P4} = boundary layer thickness according to Pohlhausen P4,

$$z_4 = \frac{\delta_{P4}^2}{\nu}\frac{U_o}{t}$$

$\lambda_{P4} = z_4 U'$ = form parameter according to Pohlhausen

$f(\lambda_{P4})$ and $g(\lambda_{P4})$ = universal functions:

$$f(\lambda) = \frac{2 - \frac{116}{315}\lambda + \left(\frac{2}{945} + \frac{1}{120}\right)\lambda^2 + \frac{2}{9072}\lambda^3}{\frac{37}{630} - \frac{\lambda}{630} - \frac{5\lambda^2}{18144}}$$

$$g(\lambda) = \frac{\frac{1}{945} + \frac{2\lambda}{9072}}{\frac{37}{630} - \frac{\lambda}{630} - \frac{5\lambda^2}{18144}}$$

Initial conditions:

At the stagnation point

$$\lambda_o = 7.052$$

that is,

$$z_{4o} = \frac{\lambda_o}{U'} = \frac{7.052}{U'} \tag{9}$$

Besides,

$$z_{40}' = -5.391 \frac{U''}{U'^2} \tag{10}$$

The isocline method was selected for the solution of the differential equation. The particular advantage of this method is that not only the initial value z_{40} is known, but that the initial inclination at the stagnation point z_{40}' also can be determined. The latter value is obtained by exact performance of the limiting process $\lim_{U \to 0} \frac{dz}{ds}$ in (8) (Howarth(6)). With z_{40}' known the integral curve passing through the initial value z_{40} is easily found which otherwise is not immediately possible because of the singularity of the Pohlhausen equation at the stagnation point.

For the profiles of the thickness $d/t = 0$, that is, for the flat plate and the circular-arc profiles, the case where the flow does not enter abruptly $(\alpha = 0)$ is exceptional since there exists no true stagnation point: the velocity at the leading edge has a finite value different from 0. The initial value of the thickness of the boundary layer is here zero, that is, at the leading edge there is:

$$z_{40} = 0 \tag{11}$$

Profile	c_a not abrupt flow entrance
0	0
200	.25
400	.5
800	1

The velocity near the leading edge of circular-arc profiles takes the same course as $\sqrt{s}$:

$$U_m = U_{oo} + C\sqrt{s} + \ldots$$

that is, U' becomes with $s \rightarrow 0$ infinite like $1/\sqrt{s}$; the velocity has a perpendicular tangent which always occurs when the contour of the profile shows a sudden change in curvature as it does here (v. Koppenfels (8)). z_4 near the leading edge for a circular-arc profile behaves like z_4 for the flat plate, that is, z_4 goes in a linear relation to s toward 0.[3] Taking these facts into consideration there results at the leading edge:

$$\lambda_o = 0; \quad z_{40}' = \frac{34.05}{U_{oo}} \tag{12}$$

It has proved advantageous to calculate the line elements z_4' directly from the equation (8) by means of a plotting of the curves $f(\lambda_{p4})$ and $g(\lambda_{p4})$. (See fig. 3.) This method is superior to the calculation of the line elements by means of the often used nomograms of Mangler (7) with respect to accuracy and its equal with respect to loss of time. Generally it will be sufficient to determine the line elements for each value of the abscissa s/t at two ordinate values only.

The boundary-layer calculation yields for each profile for a given c_a value the nondimensional boundary layer thickness z_4 and the form parameter λ_{p4} as a function of the length of the arc s along the contour. The distribution of velocity $u(y)$ in the laminar boundary layer is then obtained from:

---

[3]For the flat plate $z_4 = 34.03\ s/t$ (according to Pohlhausen (5)).

$$\frac{u}{U_m} = F_4\left(\frac{y}{\delta_{P4}}\right) + \lambda_{P4} G_4\left(\frac{y}{\delta_{P4}}\right) \tag{13}$$

with

$$\left.\begin{aligned} F_4 &= 2\frac{y}{\delta_{P4}} - 2\left(\frac{y}{\delta_{P4}}\right)^3 + \left(\frac{y}{\delta_{P4}}\right)^4 \\ G_4 &= \frac{1}{6}\frac{y}{\delta_{P4}} - \frac{1}{2}\left(\frac{y}{\delta_{P4}}\right)^2 + \frac{1}{2}\left(\frac{y}{\delta_{P4}}\right)^3 - \frac{1}{6}\left(\frac{y}{\delta_{P4}}\right)^4 \end{aligned}\right\} \tag{14}$$

The results of the boundary-layer calculation for the profiles J 800 and J 025 have been plotted as examples in figures 4 and 5: the form parameter λ_{P4} and the nondimensional displacement thickness $\frac{\delta^*}{t}\sqrt{\frac{U_o t}{\nu}}$, with δ^* standing for the displacement thickness.

The following relation exists between the displacement thickness and the boundary layer thickness according to Pohlhausen:

$$\delta^* = \delta_{P4}\left(0.3 - \frac{\lambda_{P4}}{120}\right) \tag{15}$$

The displacement thickness of the flat plate in longitudinal flow $\left(\lambda_{P4} = 0\right)$ is represented graphically in figures 4 and 5 for comparison. The following equations are valid:

$$\frac{\delta^*}{t}\sqrt{\frac{U_o t}{\nu}} = \frac{\delta^*}{\delta_{P4}}\frac{\delta_{P4}}{t}\sqrt{\frac{U_o t}{\nu}} = 0.3\sqrt{z_4} = 1.75\sqrt{\frac{s}{t}} \tag{16}$$

The profile J 800 (fig. 4) shows clearly that the displacement thickness for accelerated flow (suction side) is smaller than the displacement thickness of the flat plate whereas it is larger for retarded flow (pressure side). (Compare also fig. 16.)

From the boundary-layer calculation there result also the laminar separation points. According to the four-term method of Pohlhausen separation occurs at $\lambda_{P4} = -12$, according to the six-term method (see below) at $\lambda_{P6} = -10$ corresponding to $\lambda_{P4} = -9.63$.

Flow photographs have been taken in a Lippisch smoke tunnel for a part of the calculated profiles of models of 50-centimeter wing chord and at Re-numbers $\frac{U_o t}{\nu}$ of about 2×10^5. The points of separation have been ascertained from the flow graphs (figs. 6 to 11, appendix). Figure 12 shows the experimental and theoretical separation points for various profiles for comparison. Compare also table 3. The agreement is rather good.

After λ_{P4} has been ascertained as a function of the length of the arc s there results the instability point $(s/t)_{crit.}$ from a stability calculation (H. Schlichting (4)) based on the six-term method of Pohlhausen. The P6-method is based on a one-parameter group (parameter λ_{P6}) of boundary-layer profiles which can be represented by polynomials of the sixth degree. An investigation of stability was carried out for a number of these boundary-layer profiles in (4); first, the critical Re-number of the boundary layer $\left(\frac{U_m \delta^*}{\nu}\right)_{crit.}$ as a function of λ_{P6} was obtained. The critical Re-number of the laminar layer $\left(\frac{U_m \delta^*}{\nu}\right)_{crit.}$ as a function of λ_{P4} (fig. 13) is then immediately known also because of a universal relation between λ_{P6} and λ_{P4} indicated in (4).

Once $\lambda_{Pl_4}(s/t)$ has been ascertained from the boundary-layer calculation according to Pohlhausen's method a critical Re-number $\left(\frac{U_m\delta^*}{\nu}\right)_{crit.}$ may be coordinated to each point of the profile by means of figure 13. Moreover the Re-number of the boundary layer $\frac{U_m\delta^*}{\nu}$ can be calculated for each point of the profile at a certain $\frac{U_o t}{\nu}$:

$$\frac{U_m\delta^*}{\nu} = \frac{U_m}{U_o}\sqrt{z_4}\,\frac{\delta^*}{\delta_{Pl_4}}\sqrt{\frac{U_o t}{\nu}} \tag{17}$$

The location of the instability point is then given by

$$\frac{U_m\delta^*}{\nu} = \left(\frac{U_m\delta^*}{\nu}\right)_{crit.} \tag{18}$$

IV. RESULTS

(a) Influence of the c_a-Value and the Re-number

The results of the stability calculation, that is, the position of the theoretical instability point $\left(\frac{s}{t}\right)_{crit.}$ for the sample profiles J 800 and J 025 are plotted in figures 14 and 15 against c_a with the Re-number as parameter and furthermore against $\frac{U_o t}{\nu}$ with the c_a-value as parameter. The characteristic course of the curves is the same for all profiles; the following statements are valid: the instability point travels, with increasing c_a at a constant Re-number, forward

on the suction side, backward on the pressure side; the instability point travels forward on both suction and pressure side with increasing Re-number at a fixed c_a-value. This behavior is demonstrated very clearly in figures 16 and 17 which represent the velocity distributions for the two profiles J 800 and J 025 for the various c_a-values with instability and separation points. One can see in particular that the instability points of the suction side for Re-numbers from $\frac{U_o t}{\nu} = 10^5$ to 10^7 lie near the velocity maximum; mostly the position of the instability point for $Re = 10^6$ agrees well with the location of the velocity maximum. The pressure side of J 800 in the case where the flow does not enter abruptly ($c_a = 1$) is an exception among the above mentioned examples, since the flow from the leading edge to the center of the profile is considerably increased so that no relative velocity maximum exists. Measurements concerning the dependency of the transition point on the c_a-value were taken by A. Silverstein and J. V. Becker (9). These tests showed (as a result) the same dependency of the transition point upon the lift coefficient as the present theoretical investigations.

(b) Influence of the Camber of the Profile

The influence of the camber upon the position of the instability point can be described as follows: the instability point travels with increasing camber, at constant thickness, for all c_a-values and Re-numbers backward on the suction side, forward on the pressure side. This influence of the camber can be understood from the fact that the stagnation point and therefore the region of the accelerated stabilizing flow travels, with increasing camber, backward on the suction side whereas because of the flow around the nose of the profile a region of considerably retarded destabilizing flow originates immediately behind the nose on the pressure side. Figure 18 represents as an example the results for profiles of the thickness $d/t = 0.15$, with variable camber f/t for $c_a = 0.25$ and again the Re-number as parameter. The curves for all thicknesses and all c_a-values have the same characteristics.

(c) Influence of the Profile Thickness

The dependency of the instability point on the thickness cannot be described in such general terms as the influence of the camber since this influence depends in the following way on the c_a value: A certain "c_a not abrupt flow entrance", that is, the c_a value that corresponds to the not abrupt entering of the flow $(\alpha = 0)$ for the circular arc profile with the given camber, is coordinated to each value of the camber f/t. The curves $(s/t)_{crit.}$ versus d/t at a constant f/t show on principle two different types (fig. 19):

I. With increasing thickness, the curves $(s/t)_{crit.}$ versus d/t start from a finite value and have a flat minimum:

On the suction side for $c_a \leqq c_a$ for not abrupt flow changes.

On the pressure side for $c_a \geqq c_a$ for not abrupt flow changes.

II. The curves $(s/t)_{crit.}$ versus d/t rise starting from 0 with increasing thickness; hence, the transition point moves backward as follows:

On the suction side for $c_a > c_a$ for not abrupt flow changes.

On the pressure side for $c_a < c_a$ for not abrupt flow changes.

The results for the symmetrical profiles at $c_a = 0.25$ are represented as an example in figure 20. For the symmetrical profiles c_a for not abrupt flow changes $= 0$, that is, the dependency of the instability point on the thickness d/t for all $c_a > 0$ is of type II on the suction side, of type I on the pressure side.

The flat minimum in curves of type I does, in some cases, not exist at high Re-numbers (Re = 10^7 to 10^8), and $(s/t)_{crit.}$ versus d/t rises from the finite value $d/t = 0$.

(d) List of Tables for the Separation and Instability Point in all Joukowsky Profiles

The total result of the boundary-layer and stability calculations is represented by a graph of the curves $(s/t)_{AP\ 6}$ = const. and $(s/t)_{crit.}$ = const., respectively, in a system of axes thickness d/t - camber f/t. (See figs. 21 to 30.) A profile corresponds to each point of the plane. In particular, the symmetrical profiles are coordinated to the points of the d/t-axis, the circular arc profiles to the points of the f/t-axis, and the flat plate corresponds to the zero point. Lift coefficient and Re-number are considered as parameters. One has therewith a catalogue of Joukowsky profiles that make it possible read off, for every profile in the region $0 \leqq d/t \leqq 0.25$; $0 \leqq f/t \leqq 0/08$, the position of the separation points for $0 \leqq c_a \leqq 1$ (figs. 21 and 22) and the position of the instability point for $0 \leqq c_a \leqq 1$ and $10^5 \leqq Re \leqq 10^8$. Figures 23 to 30 represent the curves $(s/t_{crit.}$ = const. for the Reynolds numbers from $Re = \frac{U_o t}{\upsilon} = 10^5$ to 10^8 at the c_a-values $c_a = 0, 0.25, 0.5$, and 1 for suction and pressure side. For instance the values indicated in the following table for profiles of the camber f/t = 0.02 and the thickness d/t = 0.10 to 0.15 at $Re = 10^6$ and 10^7 are taken from these representations. (See page 19.)

The most remarkable matter in this graphical representation is the location of the curve $(s/t)_{AP\ 6} = 0$, and $(s/t)_{crit.} = 0$, respectively, at the various c_a-values. The position of this zero curve in the catalogue for the instability points will be discussed; the same is valid for the separation points. $(s/t)_{crit.} = 0$ can only appear for the flat plate and the circular-arc profiles on the suction side for $c_a > c_a$ for not abrupt flow changes, on the pressure side for $c_a < c_a$ for not

	$f/t = 0.02$; $d/t = 0.10$ to 0.15			
	$Re = 10^6$		$Re = 10^7$	
c_a	$(s/t)_{crit.}$ Suction side	$(s/t)_{crit.}$ Pressure side	$(s/t)_{crit.}$ Suction side	$(s/t)_{crit.}$ Pressure side
0	0.270 to 0.255	0.05 to 0.075	0.165 to 0.175	0.03 to 0.05
0.25	0.200 to 0.205	0.085 to 0.11	0.11 to 0.13	0.05 to 0.06
0.5	0.155 to 0.160	0.18 to 0.16	0.05 to 0.08	0.110 to 0.115

abrupt flow changes. The curve $(s/t)_{crit.} = 0$ always coincides with the f/t-axis; it forms a part of the f/t-axis which is determined by the actual c_a-value. Therefore no point $(s/t)_{crit.} = 0$ exists on the suction side for $c_a = 0$ since c_a for not abrupt flow changes >0 for all circular-arc profiles. For the pressure side, on the other hand, $(s/t)_{crit.} = 0$ on the whole f/t-axis. There follows in the same way for $c_a = 0.25$ that $(s/t)_{crit.} = 0$ for $0 \leq f/t < 0.02$ on the suction side and for $f/t > 0.02$ on the pressure side. Pressure and suction side, therefore, always complement each other. The point which corresponds to the circular-arc profile with $c_a = c_a$ for not abrupt flow changes (for instance J 400 at $c_a = 0.5$, compare figs. 23 to 30), that is, the end point of the distance $(s/t)_{crit.} = 0$ is a singular point in the following sense: The point itself assumes a certain value $(s/t)_{crit.}$ (different for pressure and suction side), but an infinite number of curves $(s/t)_{crit.} = \text{const.}$ which are crowding together asymptotically toward $(s/t)_{crit.} = 0$ run into it. It is true, these relations for the very thin profiles give only qualitative results from the present investigations. An additional series of thin profiles would have to be investigated in order to make more accurate statements possible. However, only profiles with thicknesses $d/t > 0.05$ which can be analyzed quantitatively, are of practical interest.

For $c_a = 0$, $(s/t)_{crit.}$ is the same on suction and pressure side for the symmetrical profiles. Therefore the curves $(s/t)_{crit.} = \text{const.}$ for suction and pressure side would adjoin at $c_a = 0$ in a joint representation of the suction and pressure side where for the pressure side the measure of the camber is directed downward. For values $c_a \neq 0$ also the curves $(s/t)_{crit.} = \text{const.}$

have continuations which correspond to the curves $(s/t)_{crit.}$ = const. for the pressure and suction side, respectively, at the appertaining c_a-value with inverted sign.

(e) Mean Value of the Laminar-Flow Distance on Suction and Pressure Side for all Joukowsky Profiles

In view of the development of laminar profiles the mean value of the laminar-flow distance on suction and pressure side is interesting. Figures 31 and 32 show the curves mean value $(\bar{s}/t)_{crit.}$ = const. in the d/t-, f/t-plane for various lift coefficients and the Re-numbers $\frac{U_o t}{\nu} = 10^6$ and 10^7 $\left[\bar{s}_{crit.} = 0.5 \left(s_{crit.\ suction} + s_{crit.\ pressure}\right)\right]$. Generally the following conclusions are valid: The profiles with the smallest mean value $(\bar{s}/t)_{crit.}$ for a certain c_a-value lie near the circular-arc profile to which this value is coordinated as c_a for not abrupt flow changes. This profile will be for $c_a = 0$ the flat plate, for $c_a = 0.25$ the profile J 200, for $c_a = 0.5$ the profile J 400 and finally for $c_a = 1$ the profile J 800. There seems to be an exceptional case at Re $\frac{U_o t}{\nu} = 10^6$ and $c_a = 0.5$ (fig. 31) which can be explained as follows: The circular-arc profile for which at the considered c_a-value the flow enters "not abruptly" (for instance J 400 at $c_a = 0.5$) is a singular point in the f/t-, d/t-diagram. Approaching this profile on the f/t-axis from two different sides one obtains two different limit values $(s/t)_{crit.}$, since once only the suction side and once only the pressure side contributes to the mean value. Only for the singular point itself suction and pressure side contribute so that this profile has a higher $(\bar{s}/t)_{crit.}$ than the

profiles on the f/t-axis near it. If one now considers the curves mean value $(\bar{s}/t)_{crit.}$ = const. for values higher than the two limit values (range I). These curves enclose the singular point and end at two points on the f/t-axis. The remaining smaller mean values $(\bar{s}/t)_{crit.}$ generally cover only a small region near the singular point (range II) where, with the present investigations as a basis, more accurate statements are not possible. Only for the case $\frac{U_o t}{\nu} = 10^6$ and $c_a = 0.5$ the range II comprises all profiles of the series considered here since on the pressure side the profile J 400 at $c_a = 0.5$ and $Re = 10^6$ has no transition point $\left[(s/t)_{crit.} = 1\right]$ and therefore the point $f/t = 0.04$ obtains a high mean value $(\bar{s}/t)_{crit.} > 0.5$. For this case there are closed curves $(\bar{s}/t)$ = const. and there exists a profile (J 115) with the smallest mean value $\left[(\bar{s}/t)_{crit.} = 0.155\right.$ at $\left.Re = 10^6.\right]$

Moreover, the following results are obtained from figures 31 and 32: All Joukowsky profiles have small mean values $(\bar{s}/t)_{crit.}$; for instance, the mean values for practically important profiles with the camber $f/t = 0.02$ and the thickness $d/t = 0.10$ to 0.20 at Re-numbers of 10^6 to 10^7 are between 0.08 and 0.2. These mean values are only to a small degree dependent on the lift coefficient; for instance, the mean values for the profile J 215 at $Re = 10^6$ and at lift coefficients $c_a = 0$ to 1 are between 0.16 and 0.175.

V. SUMMARY

A series of Joukowsky profiles with thicknesses $d/t = 0$ to 0.25 and cambers $f/t = 0$ to 0.08 was investigated with respect to the position of the instability point for various lift coefficients and Re-numbers. The following result was obtained: With

increasing Re-number, the instability point moves forward on suction and pressure side; with increasing c_a-value it moves forward on the suction side, backward on the pressure side. The position of the instability point as a function of thickness and camber of the profile is represented in the shape of a graphical list of tables which permits the reading off of the position of the instability point on suction and pressure side as well as of the mean value of the laminar-flow distance on suction and pressure side for each profile of the series.

Translated by Mary L. Mahler
National Advisory
Committee for Aeronautics

VI. REFERENCES

1. Schlichting, H.: Über die Berechnung der kritischen Reynoldsschen Zahl einer Reibungsschicht in beschleunigter und verzögerter Strömung. Jahrbuch 1940 der deutschen Luftfahrtforschung, p. I 97.

2. Pretsch, J.: Die Stabilität der Laminarströmung bei Druckgefälle und Druckanstieg. Jahrbuch 1941 der deutschen Luftfahrtforschung, p. I 58.

3. Schlichting, H.: Berechnung des Umschlagspunktes laminar/turbulent für eine ebene Platte bei kleinen Anstellwinkeln. Nicht veröffentlichter Bericht.

4. Schlichting, H., and Ulrich, A.: Zur Berechnung des Umschlagspunktes laminar/turbulent. Preisausschreiben 1940 der Lilienthal-Gesellschaft für Luftfahrtforschung. Jahrbuch 1942 der deutschen Luftfahrtforschung, p. I 8.

5. Pohlhausen, K.: Zur näherungsweisen Integration der Differentialgleichung der laminaren Reibungsschicht. Z. angew. Math. u. Mech. Bd. 1, p. 252, 1921.

6. Howarth, L.: On the Calculation of Steady Flow in the Boundary Layer Near the Surface of a Cylinder in a Stream. ARC Rep. 1632 (1935).

7. Mangler, W.: Einige Nomogramme zur Berechnung der laminaren Reibungsschicht an einem Tragflügelprofil. Jahrbuch 1940 der deutschen Luftfahrtforschung p. I 16.

8. Koppenfels, W. v.: Two-Dimensional Potential Flow Past a Smooth Wall with Partly Constant Curvature. NACA TM 996, 1941.

9. Silverstein, A., and Becker, J. V.: Determinations of Boundary-Layer Transitions on Three Symmetrical Airfoils in the NACA Full-Scale Wind Tunnel. NACA-Rep. No. 637 (1938).

10. Holstein, H., and Bohlen, T.: Ein vereinfachtes Verfahren zur Berechnung laminarer Reibungsschichten, die dem Näherungsansatz von K. Pohlhausen genügen (noch nicht veröffentlicht).

TABLE 1

PROFILE CONSTANTS (COMMENTS SEE PARAGRAPH III (a))

Profile	ε_1 (1)	ε_4	β (deg)	$\frac{1}{2\pi}\left(\frac{dc_a}{da}\right)_{c_a=0}$	$\frac{t}{a}$	$\frac{t'}{t}$ Suction side	$\frac{t'}{t}$ Pressure side	$\frac{\rho}{t}$	$\frac{\rho/t}{(d/t)^2}$ (2)
000	0	0	0	1	4	1	1	0	1.183
005	.041	0	0	1.0394	4.006	1.007	1.007	.0031	1.180
010	.083	0	0	1.0765	4.024	1.016	1.016	.0116	1.172
015	.131	0	0	1.1159	4.054	1.028	1.028	.0258	1.150
020	.183	0	0	1.1547	4.098	1.045	1.045	.0447	1.118
025	.240	0	0	1.1934	4.156	1.069	1.069	.0674	1.083
200	0	.040	2.3	1.0008	4	1.002	1.0015	0	
205	.041	.040	2.3	1.0402	4.006	1.013	1.006	.0031	
210	.083	.040	2.3	1.0774	4.024	1.025	1.009	.0116	
215	.131	.040	2.3	1.1168	4.054	1.041	1.016	.0258	
220	.185	.040	2.3	1.1556	4.098	1.057	1.028	.0447	
225	.240	.040	2.3	1.1944	4.156	1.077	1.059	.0674	
400	0	.080	4.6	1.8032	4	1.004	1.004	0	
405	.041	.080	4.6	1.0427	4.006	1.0185	1.0055	.0031	
410	.083	.080	4.6	1.0799	4.024	1.033	1.008	.0116	
415	.131	.080	4.6	1.1195	4.054	1.049	1.012	.0258	
420	.183	.080	4.6	1.1584	4.098	1.066	1.0215	.0447	
425	.240	.080	4.6	1.1972	4.156	1.085	1.0515	.0674	
800	0	.162	9.2	1.0131	4	1.017	1.017	0	
805	.041	.162	9.2	1.0530	4.006	1.029	1.015	.0031	
810	.083	.162	9.2	1.0906	4.024	1.042	1.014	.0116	
815	.131	.162	9.2	1.1305	4.054	1.058	1.016	.0258	
820	.183	.162	9.2	1.1698	4.098	1.077	1.023	.0447	
825	.240	.162	9.2	1.2090	4.156	1.126	1.042	.0674	

Annotations to table 1:

[1]The profile thicknesses d/t determined by the parameter values ε_1 do not agree quite exactly with the thickness indicated by the profile type. The exact values of d/t are obtained by calculation of the profile contour according to equation (1) with its values of ε_1 and ε_4.

[2]There is valid $\varepsilon_1 \rightarrow 0$: $\frac{d}{t} = \frac{3}{4}\sqrt{3}\,\varepsilon_1$.

TABLE 2

THEORETICAL ANGLE OF ATTACK α (DEGREE)

C_a	Profile					
	000	005	010	015	020	025
0	0	0	0	0	0	0
.25	2.3	2.2	2.1	2.05	2.0	1.9
.5	4.6	4.4	4.2	4.1	4.0	3.8
1	9.2	8.8	8.4	8.2	8.0	7.6
C_a	200	205	210	215	220	225
0	-2.3	-2.3	-2.3	-2.3	-2.3	-2.3
.25	0	-.1	-.2	-.25	-.3	-.4
.5	2.3	2.1	1.9	1.8	1.7	1.5
1	6.9	6.5	6.2	5.9	5.6	5.4
C_a	400	405	410	415	420	425
0	-4.6	-4.6	-4.6	-4.6	-4.6	-4.6
.25	-2.3	-2.4	-2.5	-2.55	-2.6	-2.7
.5	0	-.2	-.4	-.5	-.7	-.8
1	4.6	4.2	3.9	3.5	3.3	3.1
C_a	800	805	810	815	820	825
0	-9.2	-9.2	-9.2	-9.2	-9.2	-9.2
.25	-6.9	-7.0	-7.1	-7.2	-7.25	-7.3
.5	-4.6	-4.9	-5.0	-5.2	-5.3	-5.4
1	0	-.5	-.8	-1.1	-1.4	-1.6

TABLE 3

LAMINAR SEPARATION POINTS; COMPARISON OF TEST AND CALCULATION

S = Suction side, D = Pressure side

		C_a	0	0.25	0.5	0.75	1
J 400	Theor.	S	0.929	0.891	0.835	0	0
		D	0	0			
	Exper.	S	.92	.88	.83	.75	0
		D	0	0			
J 800	Theor.	S	.8925	.86	.8275		.755
		D	0	0	0	0	
	Exper.	S	.88	.84	.80	.76	.73
		D	0	0	0	0	
J 005	Theor.	S	.997	.6596			
		D	.997				
	Exper.	S		.70	.28	.10	.015
		D					
J 025	Theor.	S	.4025	.3533	.308		.252
		D	.4025	.4345	.491		.592
	Exper.	S	.45	.42	.385	.36	.32
		D	.45	.485	.54	.60	.68
J 415	Theor.	S	.686	.630	.570		.476
		D	.200	.283	.377		.494
	Exper.	S	.95	.86	.73	.65	.63
		D	.19	.29	.31	.33	.48
J 815	Theor.	S	.737	.685	.648		.594
		D	.0427	.0562	.0934		.1924
	Exper.	S	.86	.78	.71	.67	.63
		D	.06	.075	.10	.12	.16

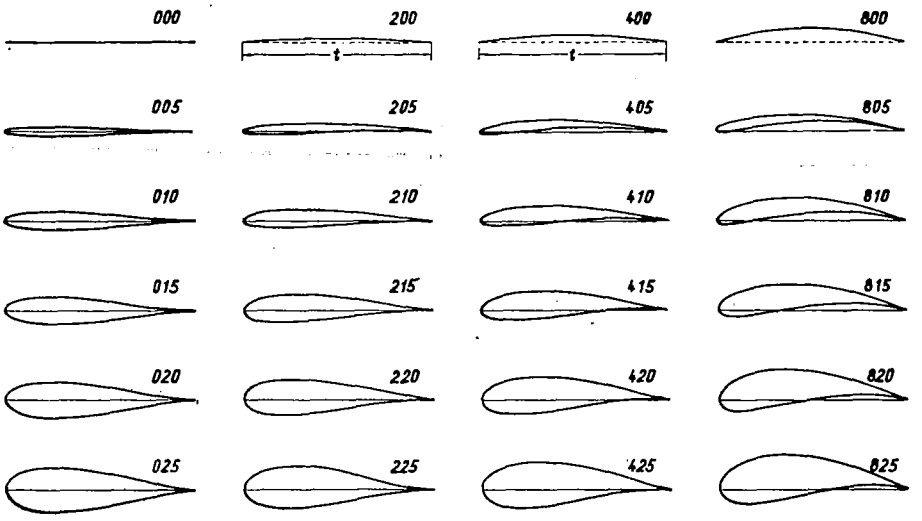

Figure 1.- Joukowsky profiles: thickness d/t = 0 to 0.25; camber f/t = 0 to 0.08. Profile number: for instance, J 415 stands for the Joukowsky profile with f/t = 0.04 and d/t = 0.15.

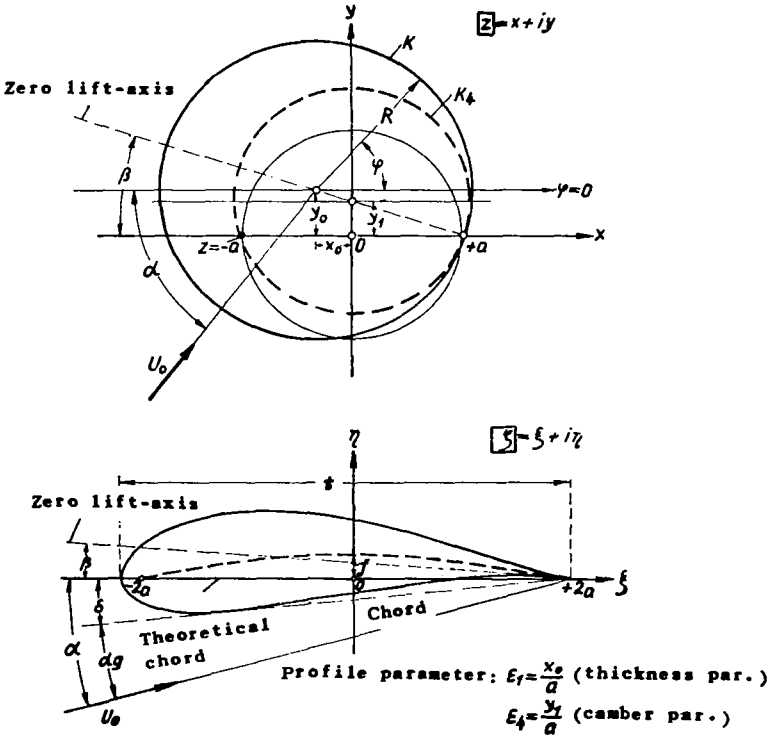

Figure 2.- Explanatory sketch to the Joukowsky transformation (schematic).

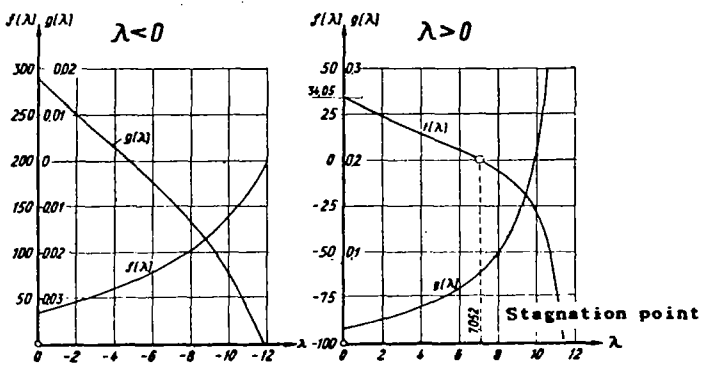

Figure 3.- Auxiliary function $f(\lambda_{P4})$ and $g(\lambda_{P4})$ for the boundary-layer calculation.

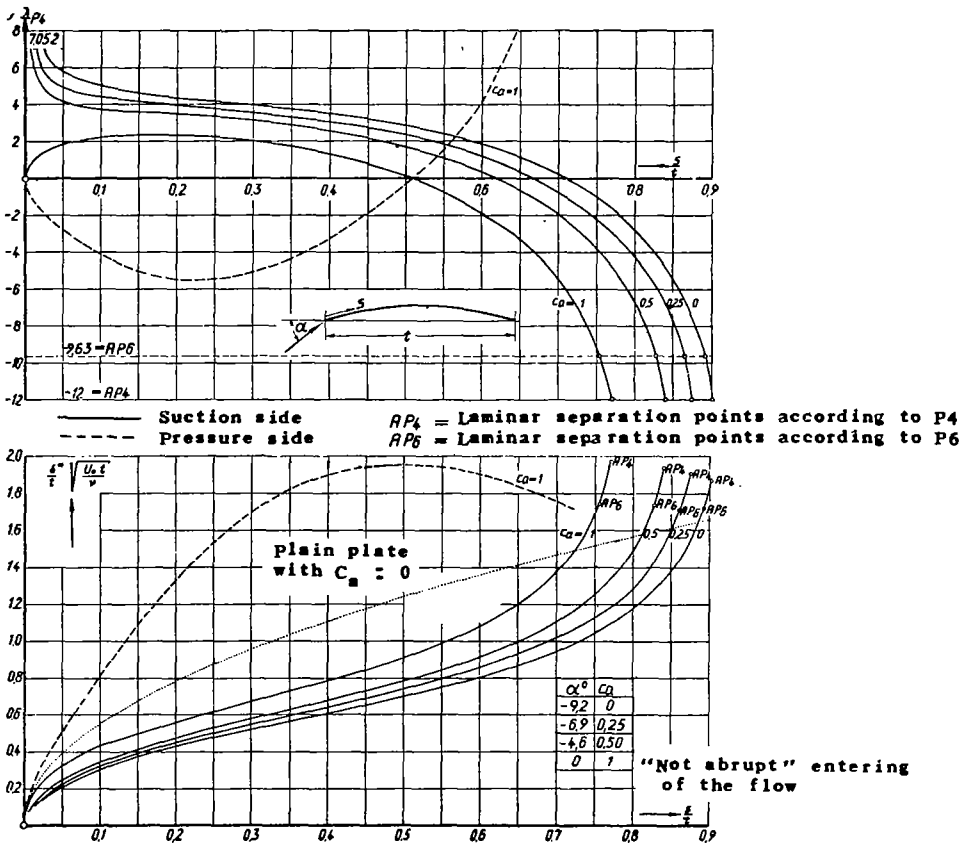

Figure 4.- Profile J 800, boundary-layer calculation: form parameter λ_{P4} and displacement thickness $\frac{\delta^*}{t}\sqrt{\frac{U_0 t}{\nu}}$.

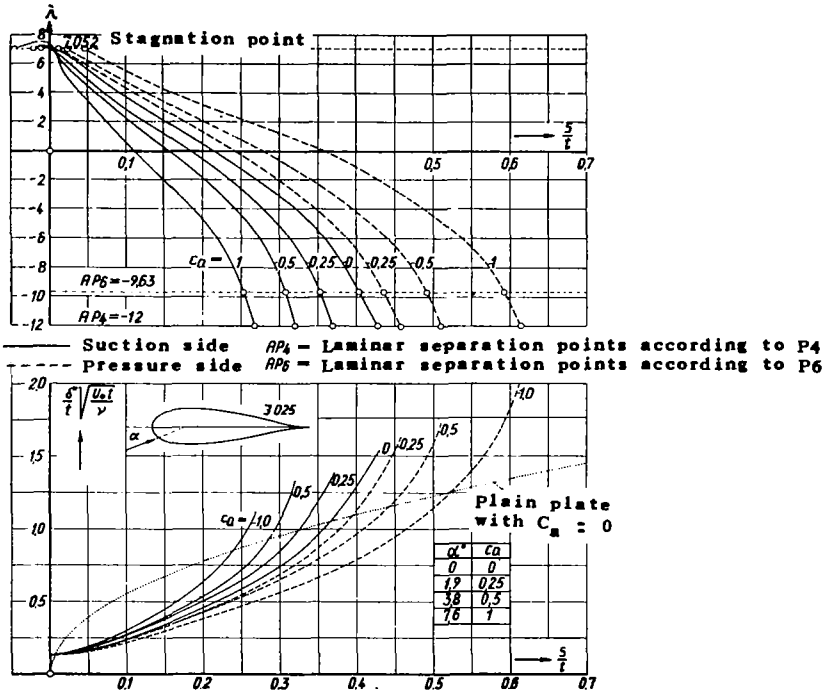

Figure 5.- Profile J 025, boundary-layer calcualtion: form parameter λ_{P4} and displacement thickness $\frac{\delta^*}{t}\sqrt{\frac{U_0 t}{\nu}}$.

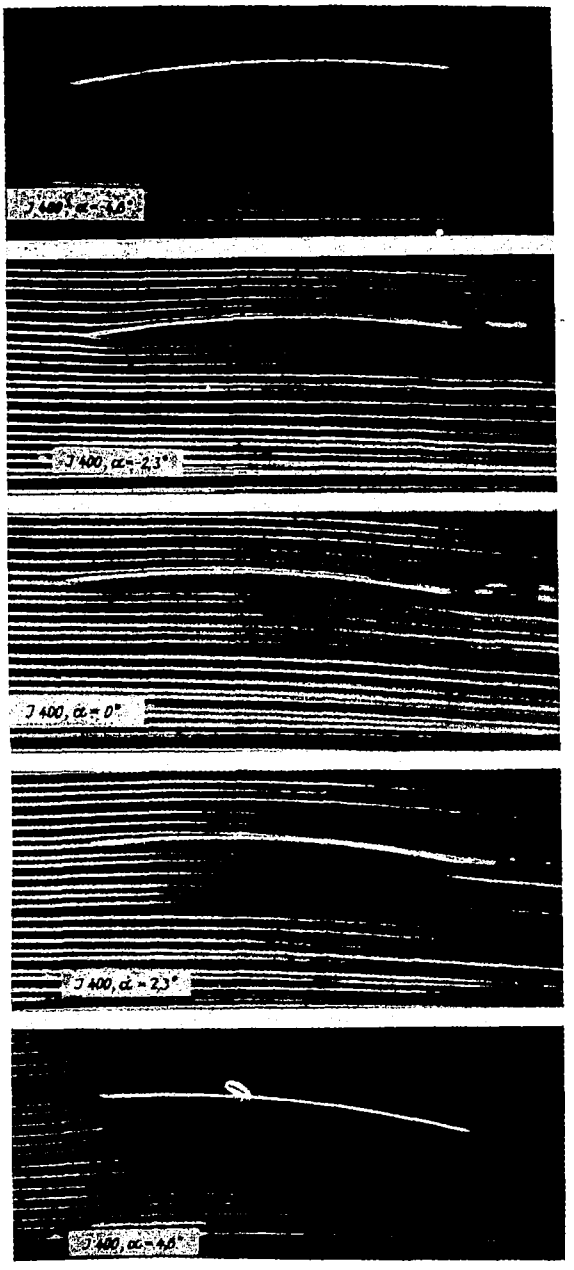

α°	Ca theor.
—4,6	0
—2,3	0,25
0	0,50*)
2,3	0,75
4,6	1,00

Figure 6. Profile J 400, smoke tunnel photographs (Re = 2. 10^5).
*) not abrupt entering.

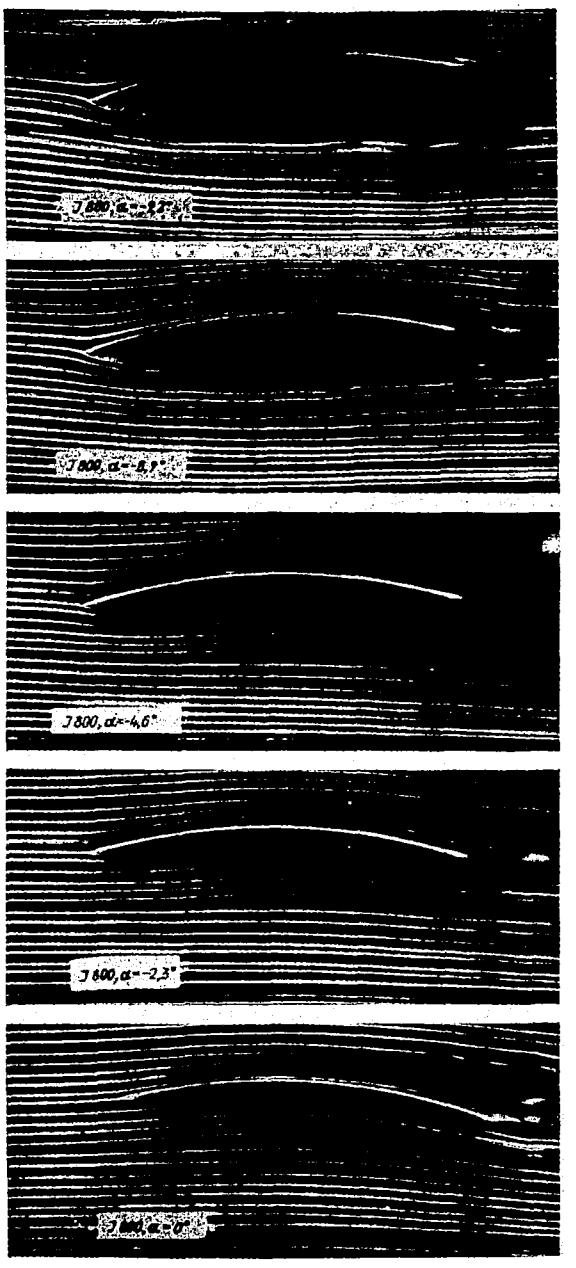

α°	Ca theor.
—9,2	0
—6,9	0,25
—4,6	0,50
—2,3	0,75
0	1,00*)

Figure 7. Profile J 800, smoke tunnel photographs (Re = 2. 10^5). Laminar separation points see Fig. 12.
*) not abrupt entering.

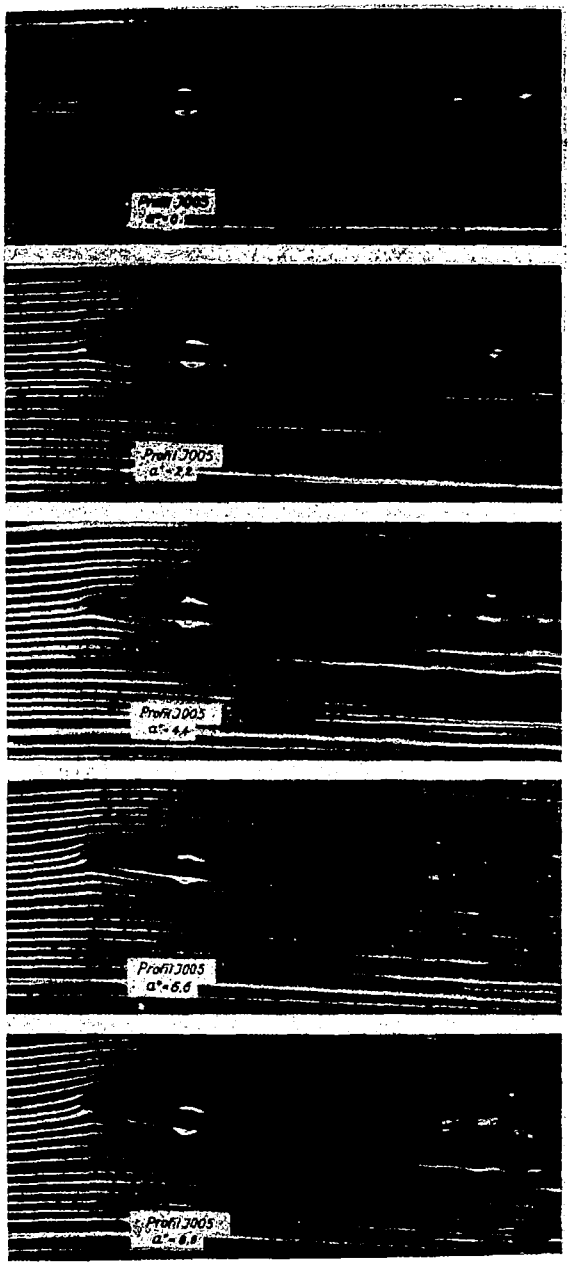

α^0	C_a theor.
0	0
2,2	0,25
4,4	0,50
6,6	0,75
8,8	1,00

Figure 8. Profile J 005, smoke tunnel photographs (Re = 2.10^5).

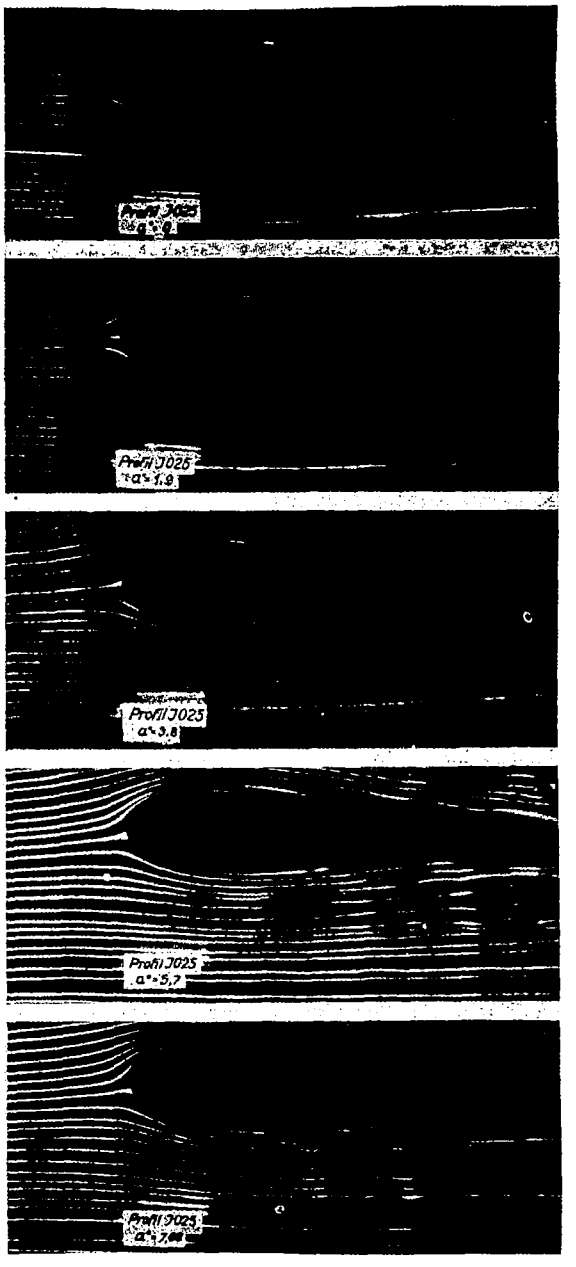

α^0	C_a theor
0	0
1,9	0,25
3,8	0,50
5,7	0,75
7,65	1,00

Figure 9. Profile J 025, smoke tunnel photographs (Re = 2.10^5). Laminar separation points see Fig. 12.

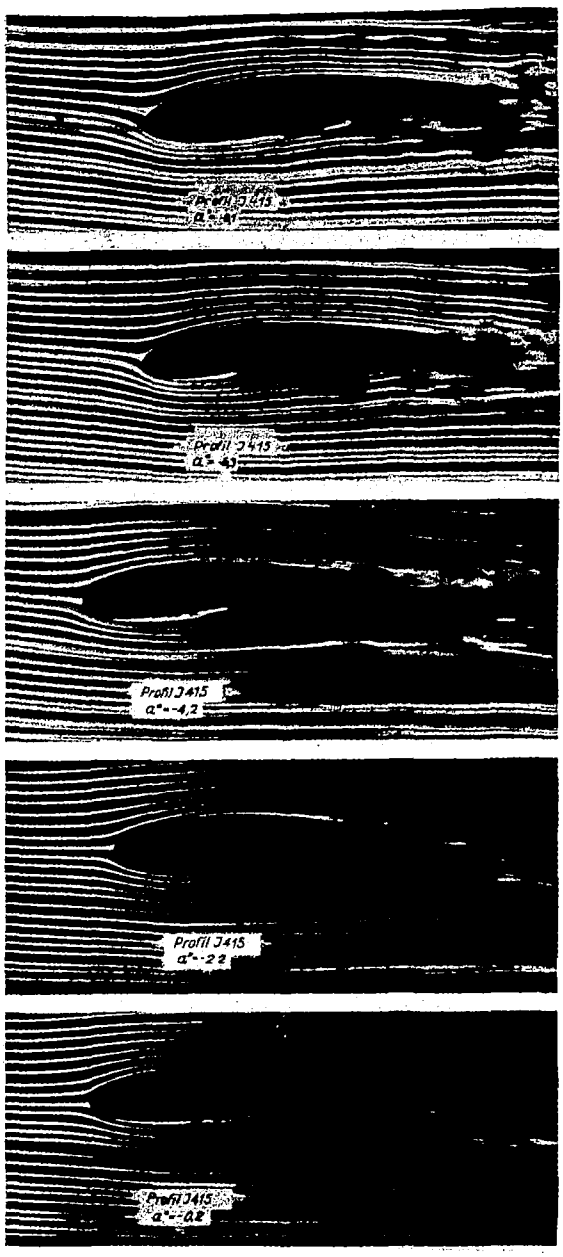

α^0	$\alpha_g{}^0$	C_{rt} theor.
—4,6	—8,1	0
—2,5	—6,3	0,25
—0,5	—4,2	0,50
1,45	—2,2	0,75
3,5	—0,2	1,00

Figure 10. Profile J 415, smoke tunnel photographs (Re = 2.10^5). Definitions of α and α_g see Fig. 2.

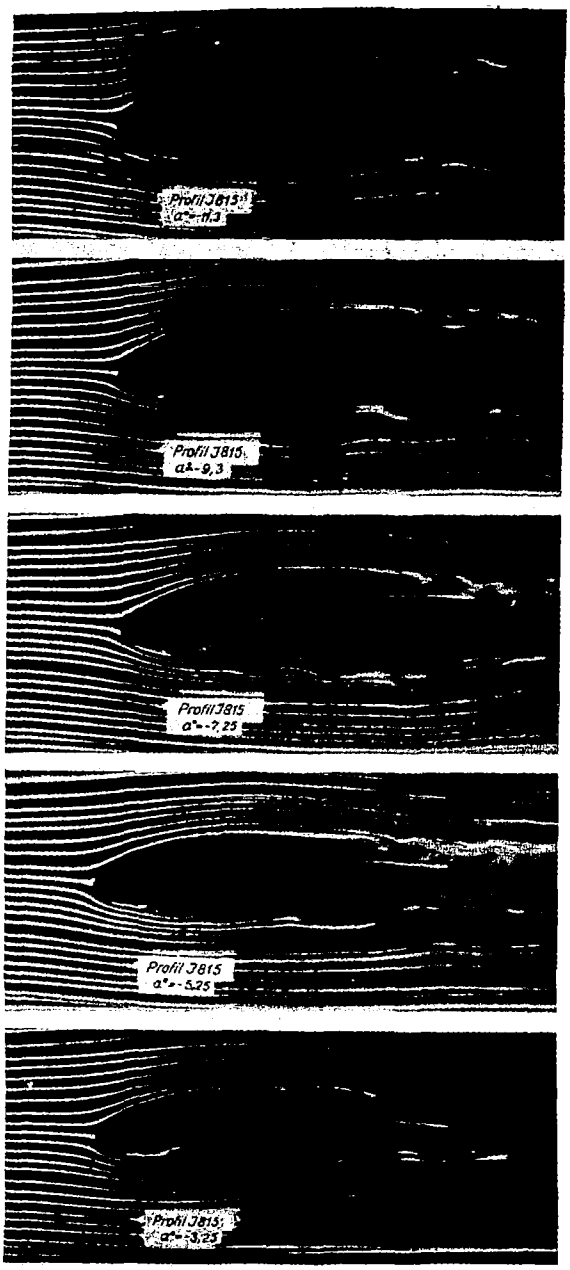

α^0	$\alpha_g{}^0$	C_{rt} theor.
—9,2	—11,3	0
—7,2	— 9,3	0,25
—5,7	— 7,25	0,50
—3,2	— 5,25	0,75
—1,1	— 3,25	1,00

Figure 11. Profile J 815, smoke tunnel photographs (Re = 2.10^5). Laminar separation points see Fig. 12.

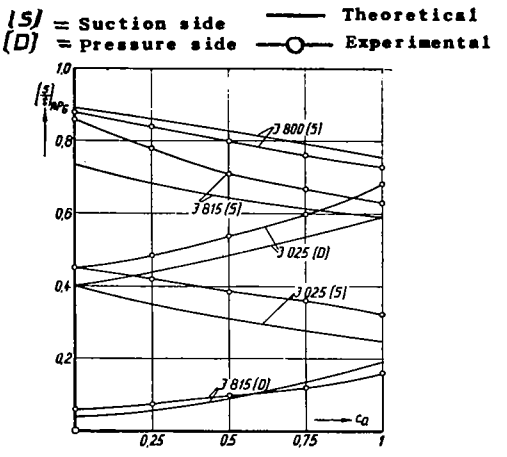

Figure 12.- Laminar separation points A P_6 versus c_a, comparison of test and calculation for the profiles J 800, J 025, and J 815.

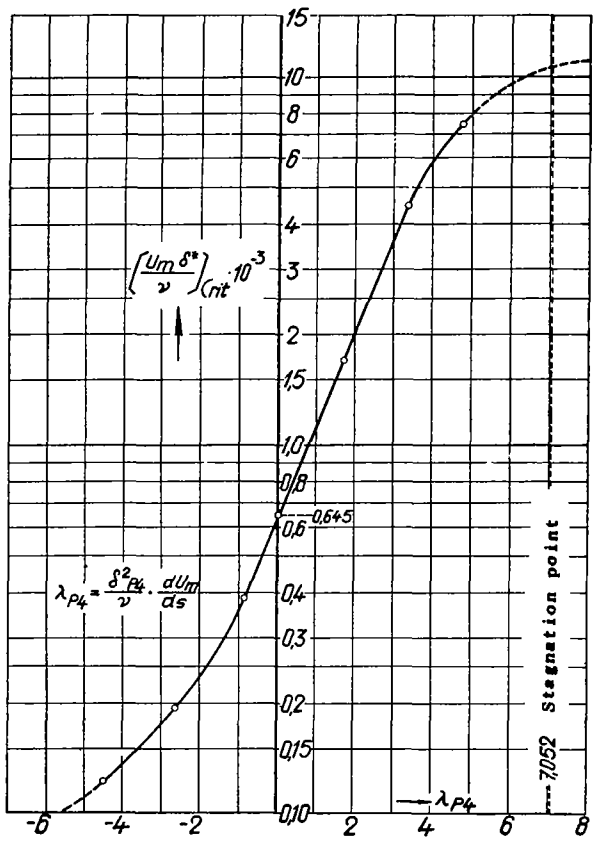

Figure 13. Universal relation between the critical Reynolds number $\left(\frac{U_m \delta^*}{\nu}\right)_{crit}$ and the form parameter λ_{P4}.

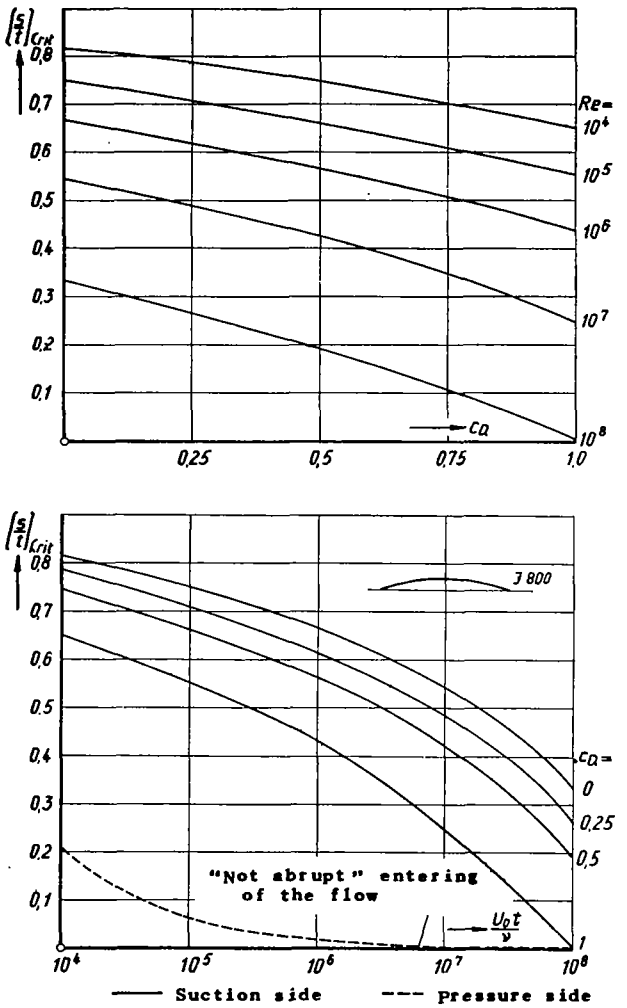

Figure 14.- Profile J 800: Result of the stability calculation, $(\frac{s}{t})_{crit}$, versus $\frac{U_0 t}{\nu}$ and c_a.

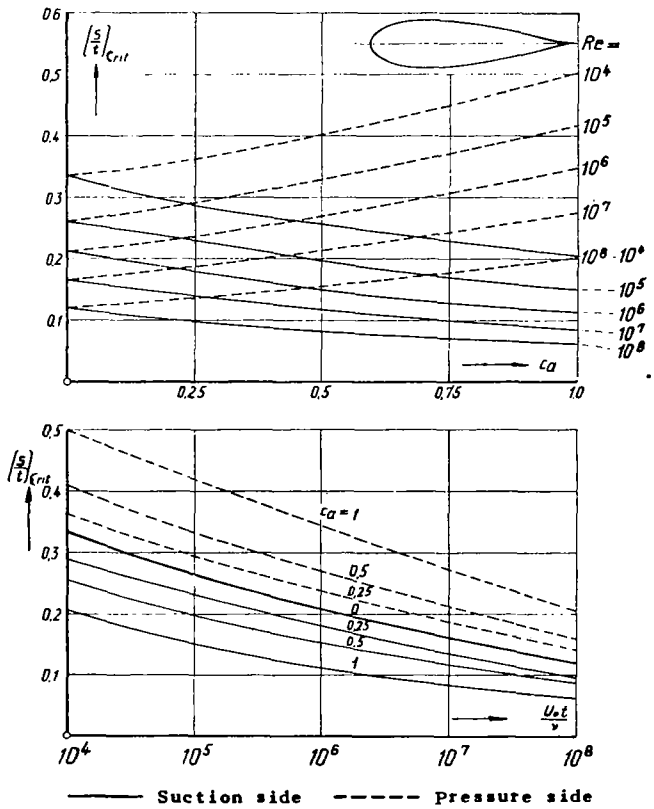

Figure 15.- Profile J 025: Result of the stability calculation, $\left(\frac{s}{t}\right)_{crit.}$ versus $\frac{U_o t}{\upsilon}$ and c_a.

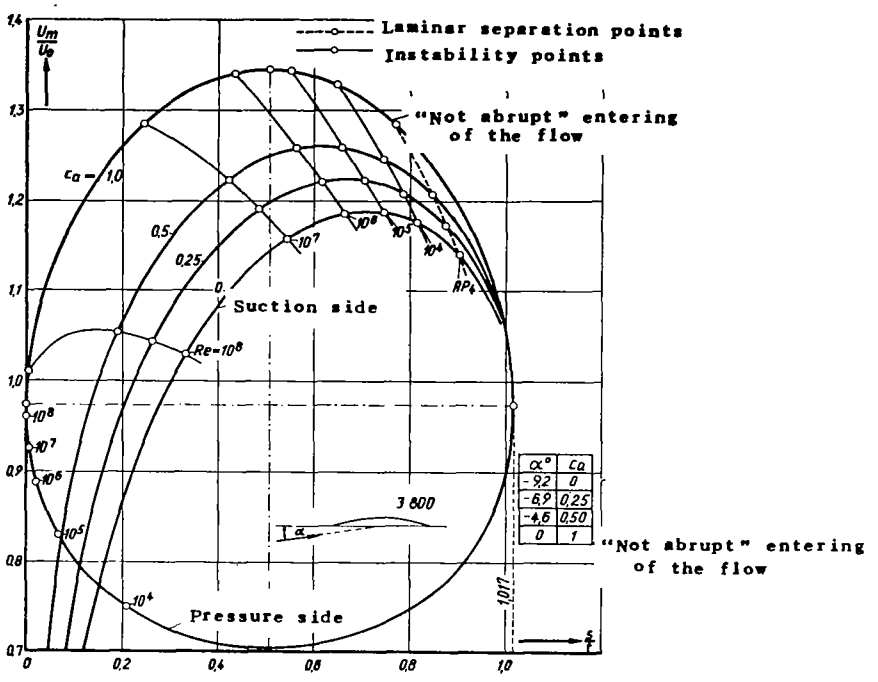

Figure 16.- Profile J 800: Velocity distribution with instability and separation points at various $Re = \frac{U_o t}{\nu}$ and c_a - values.

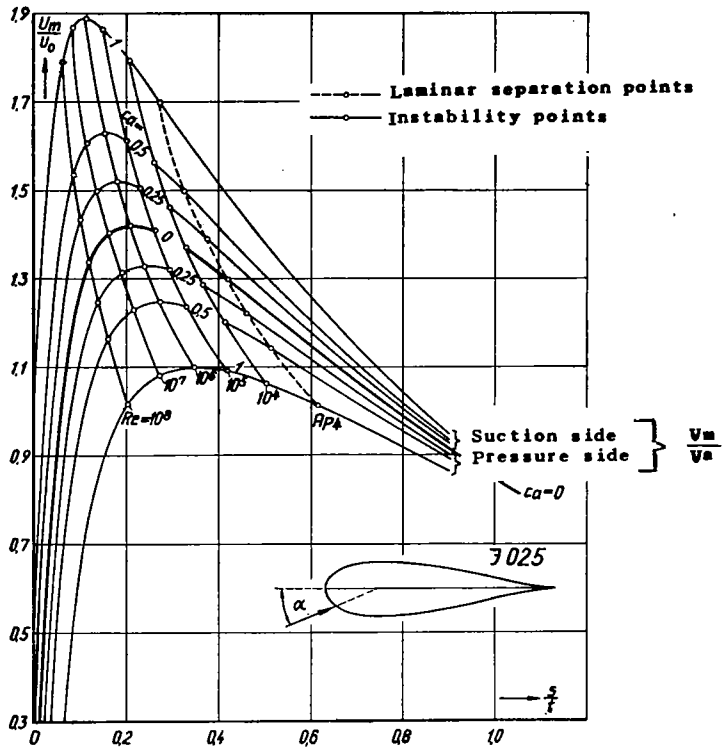

Figure 17.- Profile J 025: Velocity distribution with instability and separation points at various $Re = \frac{U_o t}{\nu}$ and c_a - values.

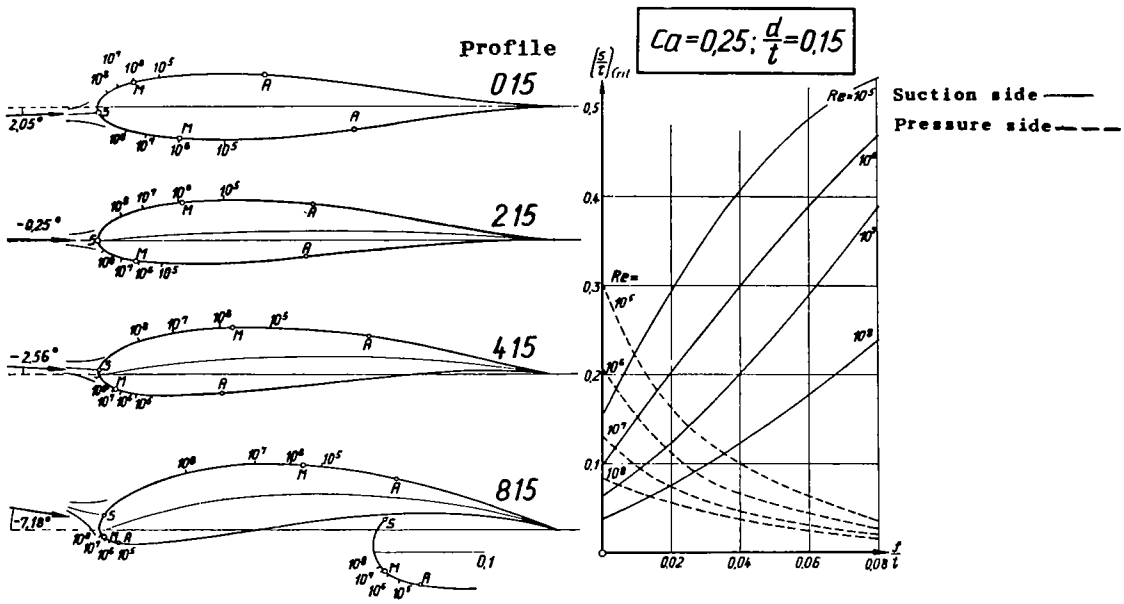

Figure 18.- Influence of the camber upon the position of the instability point for profiles of the thickness d/t = 0.15 with c_a = 0.25. A = laminar separation point; M = maximum velocity; S = stagnation point.

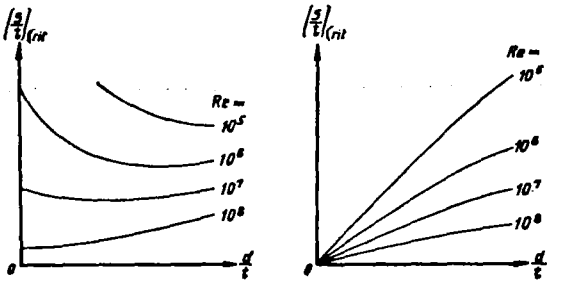

Figure 19.- Characteristics curves about the influence of the thickness of profile upon the position of the instability point. Suction side: $c_a \leqq c_a$ for not abrupt flow changes; suction side: $c_a > c_a$ for not abrupt flow changes; pressure side: $c_a \geqq c_a$ for not abrupt flow changes; pressure side: $c_a < c_a$ for not abrupt flow changes.

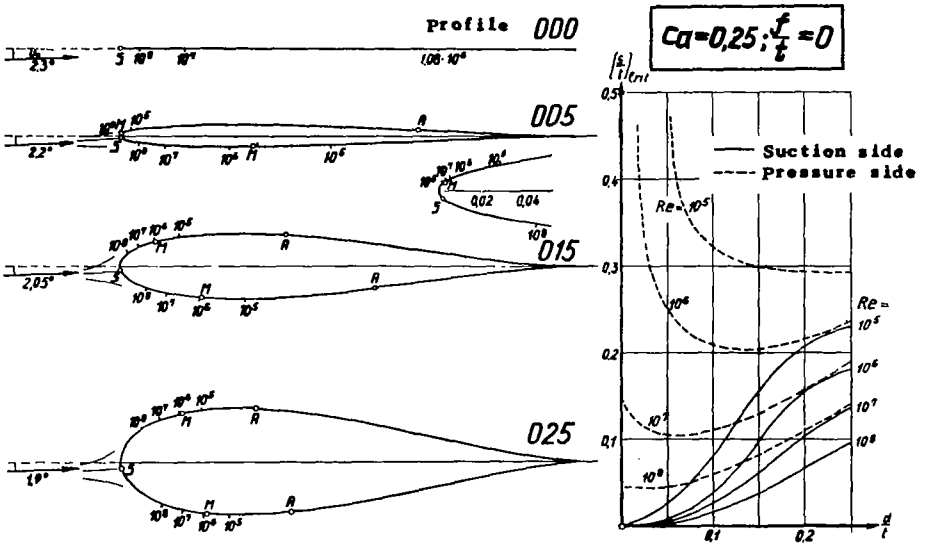

Figure 20.- Influence of the thickness of the profile upon the position of the instability point for symmetrical profiles with $c_a = 0.25$. A = laminar separation point; M = maximum velocity; S = stagnation point.

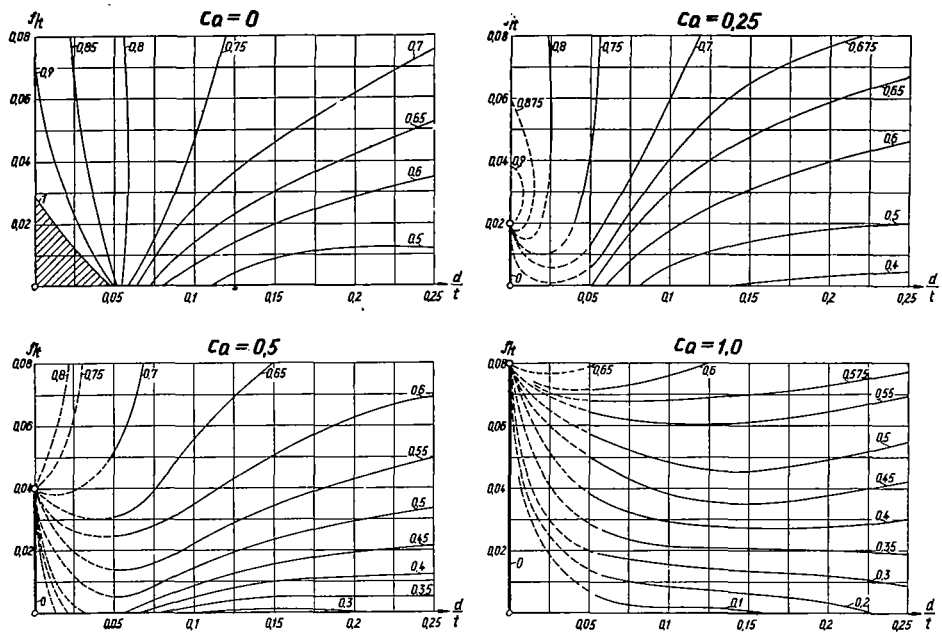

Figure 21.- Position of the laminar separation point $(s/t)_{AP\ 6}$ as a function of the thickness of the profile d/t and the camber of the profile f/t; suction side.

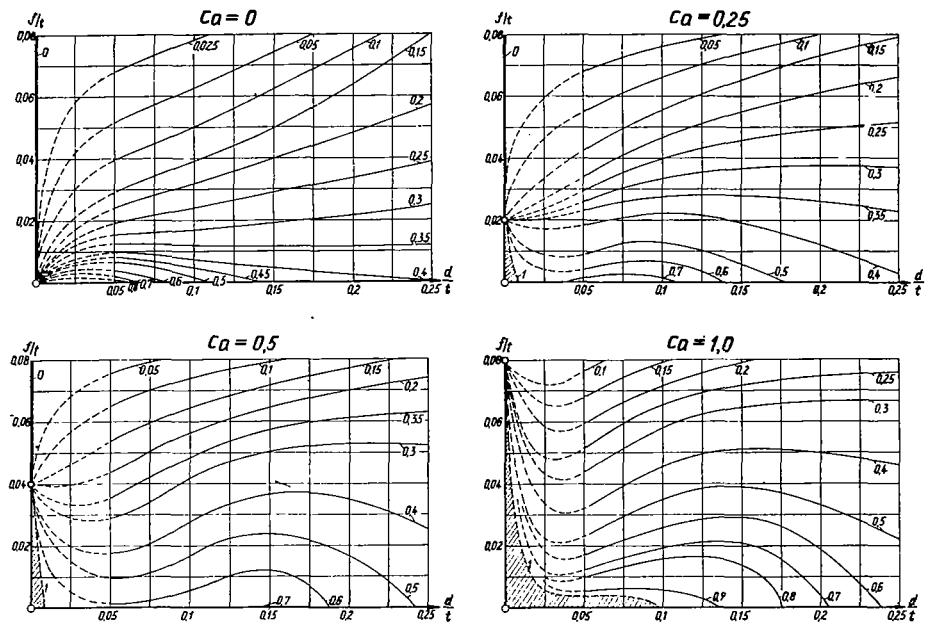

Figure 22.- Position of the laminar separation point $(s/t)_{AP\ 6}$ as a function of the thickness of the profile d/t and the camber of the profile f/t; pressure side.

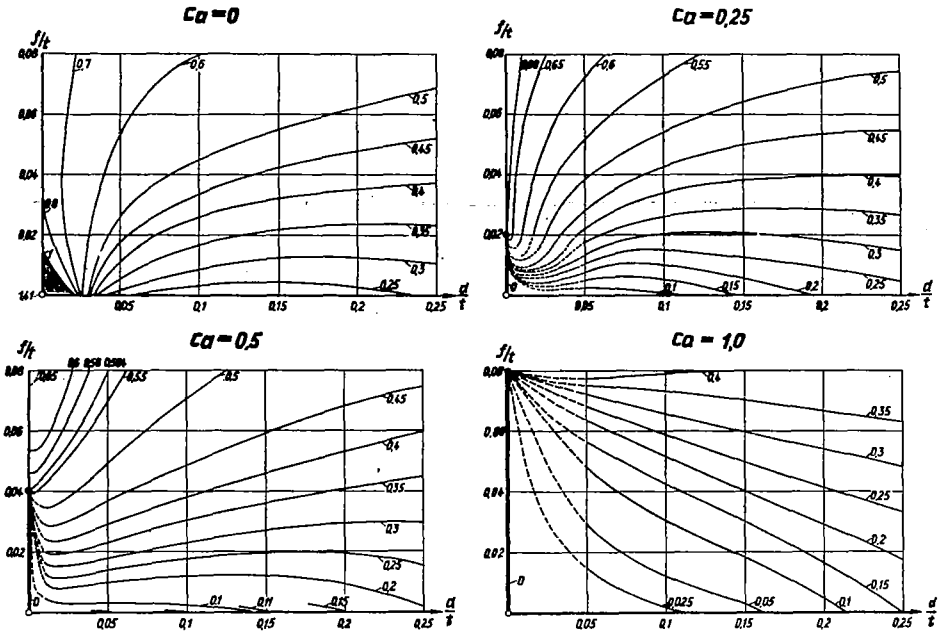

Figure 23.- Position of the instability point $(s/t)_{crit.}$ as a function of the thickness of the profile d/t and the camber of the profile f/t; suction side; $Re = 10^5$.

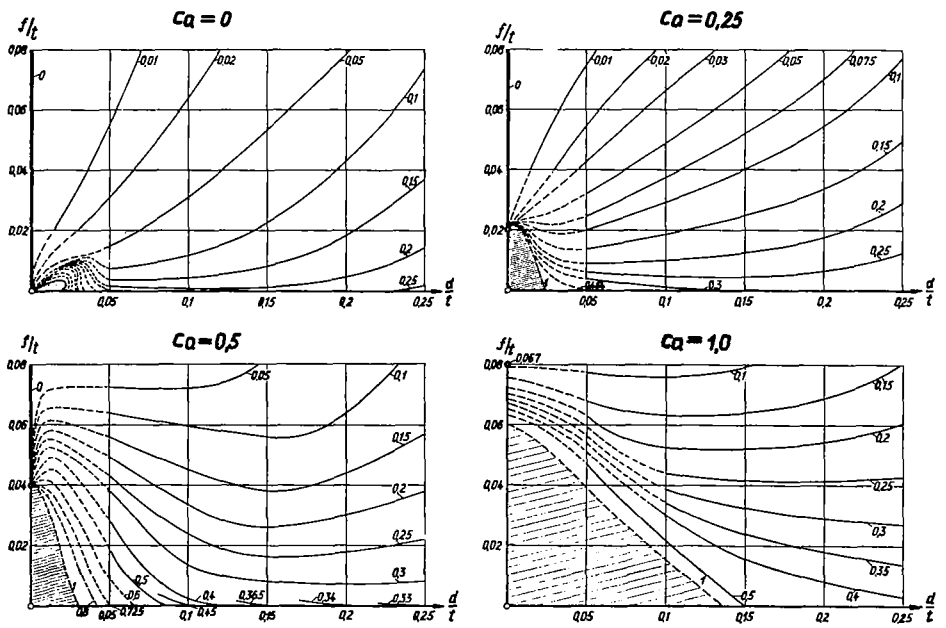

Figure 24.- Position of the instability point $(s/t)_{crit.}$ as a function of the thickness of the profile d/t and the camber of the profile f/t; pressure side; $Re = 10^5$.

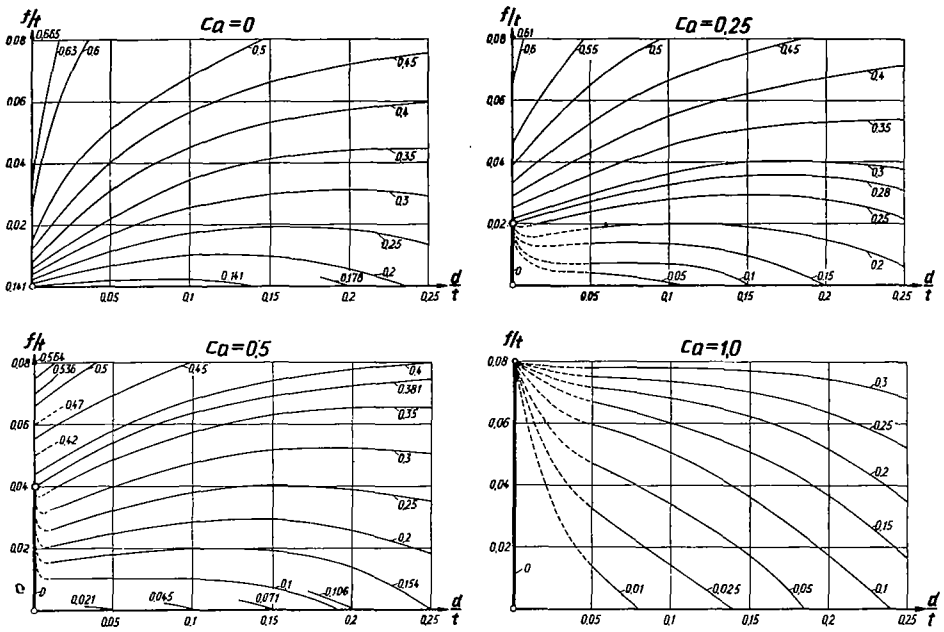

Figure 25.- Position of the instability point $(s/t)_{crit.}$ as a function of the thickness of the profile d/t and the camber of the profile f/t; suction side; $Re = 10^6$

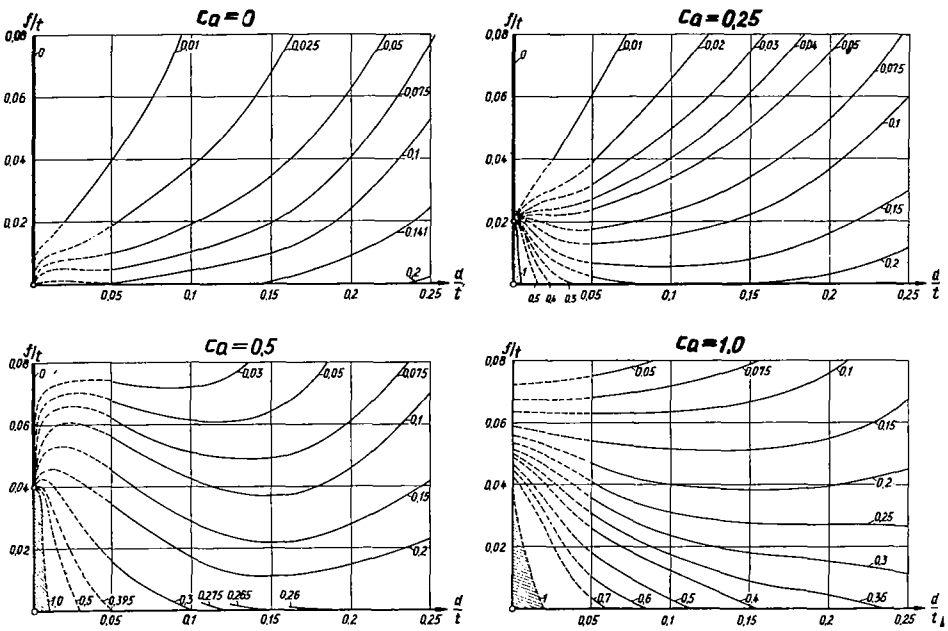

Figure 26.- Position of the instability point $(s/t)_{crit.}$ as a function of the thickness of the profile d/t and the camber of the profile f/t; pressure side; $Re = 10^6$.

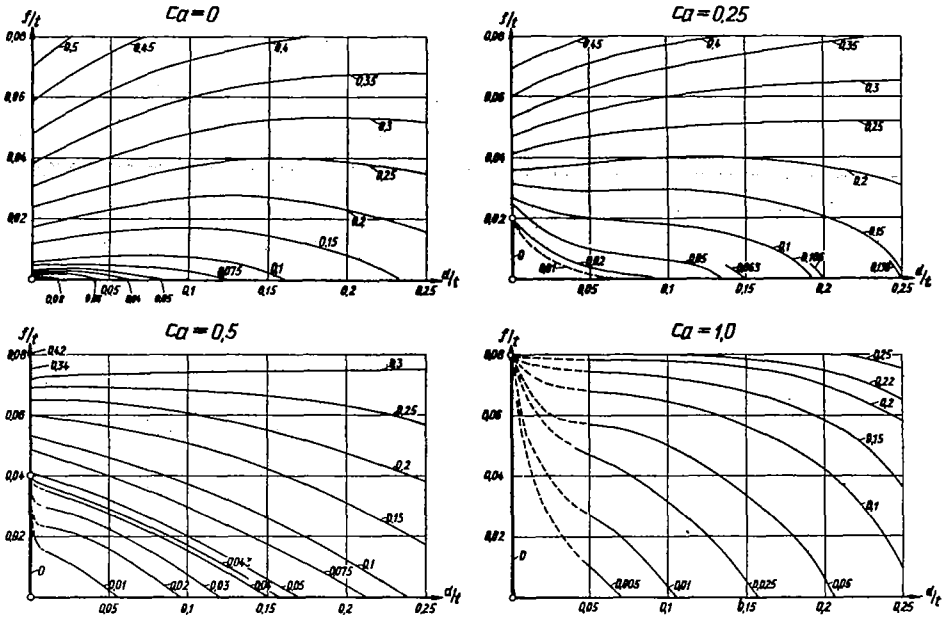

Figure 27.- Position of the instability point $(s/t)_{crit.}$ as a function of the thickness of the profile d/t and the camber of the profile f/t; suction side; $Re = 10^7$.

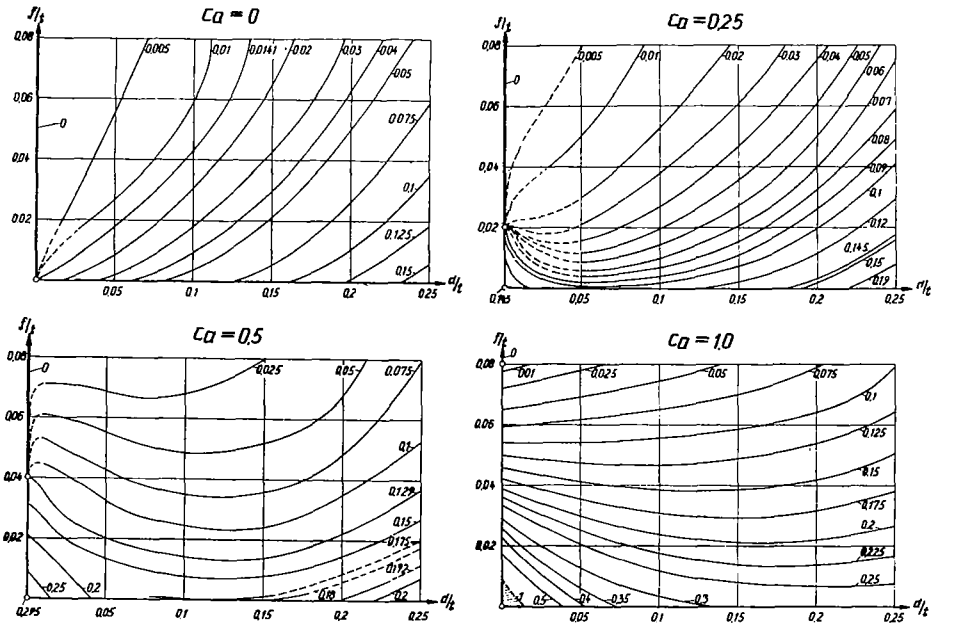

Figure 28.- Position of the instability point $(s/t)_{crit.}$ as a function of the thickness of the profile d/t and the camber of the profile f/t; pressure side; $Re = 10^7$.

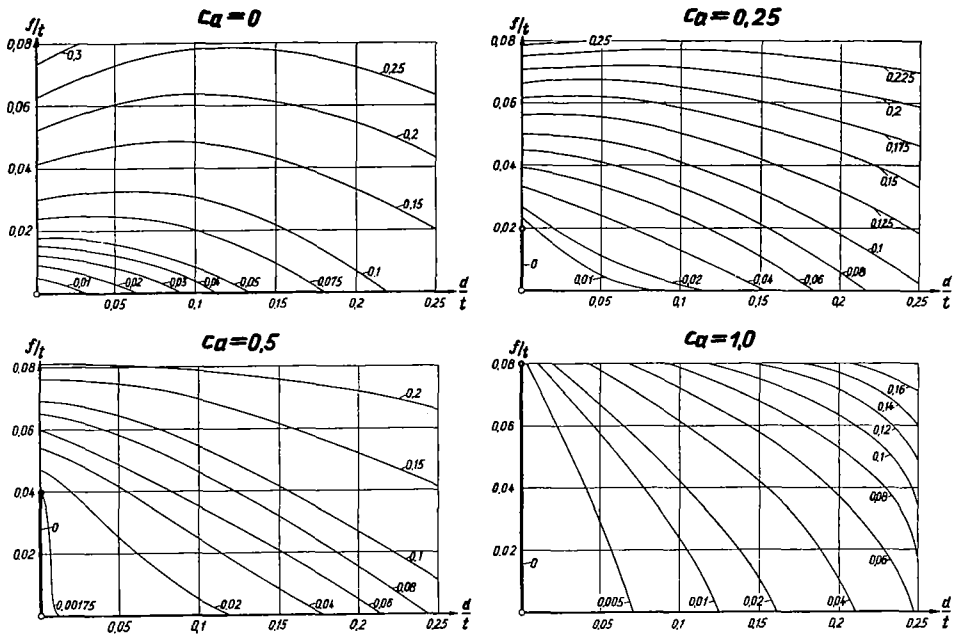

Figure 29.- Position of the instability point $(s/t)_{crit.}$ as a function of the thickness of the profile d/t and the camber of the profile f/t; suction side; $Re = 10^8$

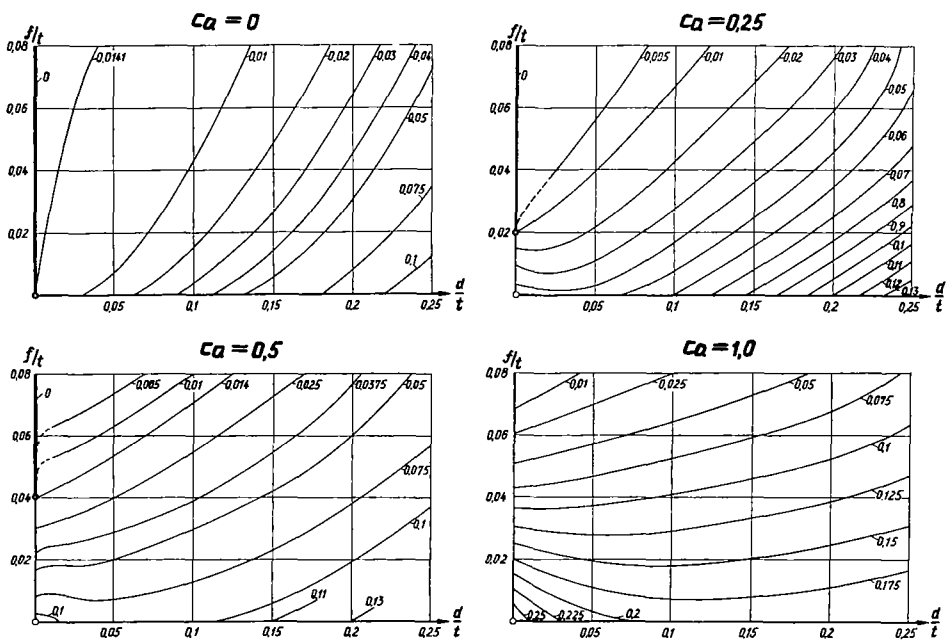

Figure 30.- Position of the instability point $(s/t)_{crit.}$ as a function of the thickness of the profile d/t and the camber of the profile f/t; pressure side; $Re = 10^8$.

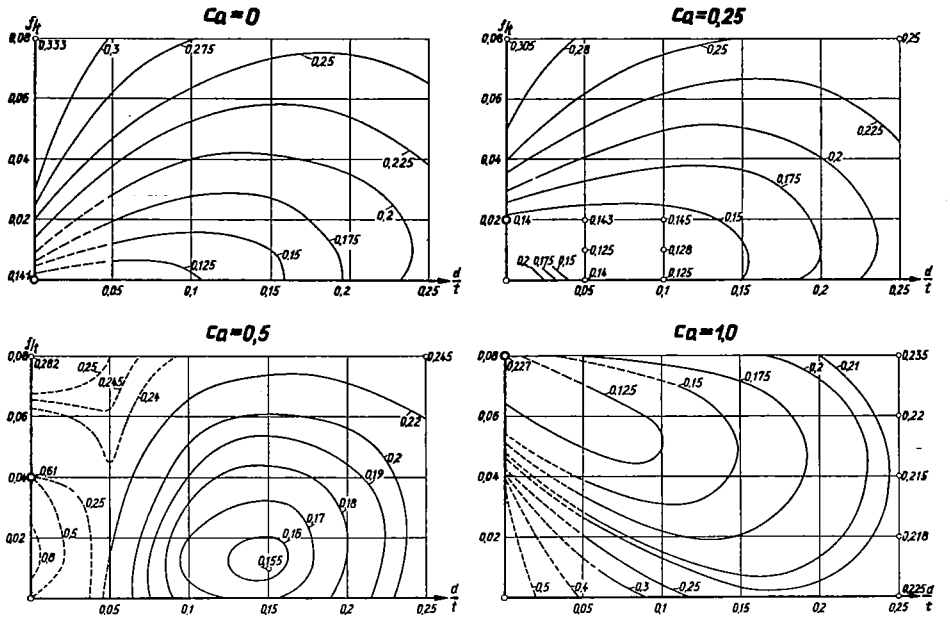

Figure 31.- Mean position of the instability point $(\bar{s}/t)_{crit.}$ for pressure and suction side at $Re = 10^6$. $(\bar{s})_{crit.} = 1/2\ (s_{crit.\ suct.\ side} + s_{crit.\ pressure\ side})$.

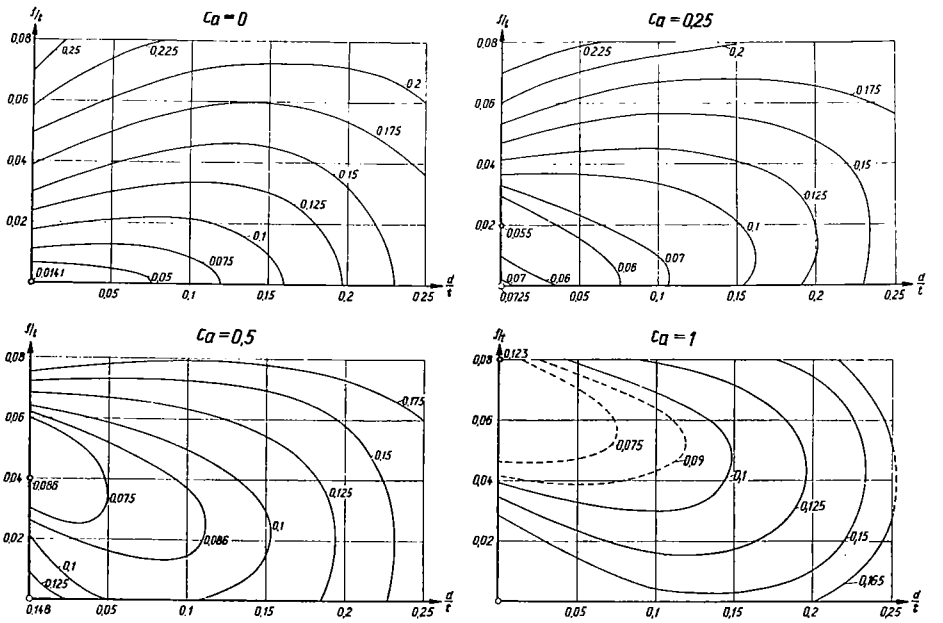

Figure 32.- Mean position of the instability point $(\bar{s}/t)_{crit.}$ for pressure and suction side at $Re = 10^7$. $(s)_{crit.} = 1/2\ (s_{crit.\ suct.\ side} + s_{crit.\ pressure\ side})$.

LANGLEY RESEARCH CENTER
3 1176 00520 3105